The Relative Impact of Urbanization Expansion and Climate Change on Flood Hazard in Amman City

Ibrahim M. Oroud*

Mutah University, Karak, Jordan

Abstract

The effect of land use changes and climate change on flooding frequency and magnitude was evaluated in the rapidly expanding Amman City, Jordan. A high spatial resolution hydrological model was run on a daily timestep from 1985 through 2021 to simulate the evolution of flooding events using three land use scenarios, 1986, 2001, and 2024. Land use derived from Landsat images indicated a large urban expansion, with urban areas expanding from ~83 km^2 in 1986 to 137 km^2 in 2024. Simulation results were commensurate with observed and archived datasets. Aridification and warming were observed in the study area. Precipitation decreased and the minimum and maximum temperatures rose significantly during the past 20 years. It is expected that aridification and warming will provide a buffering effect on flooding events, but the effect of urbanization is far more important in increasing flooding hazards as demonstrated by the frequency and magnitude of flooding events during recent years. The rapid urban expansion altered the ability of the surface to absorb and retain rainwater, leading to recurrent severe flooding events in recent years as revealed by the frequency of reported flooding events and the simulation results. The simulated average annual surface runoff for the 1986 land use scenario from 1985 to 2021 was 71 mm, whereas its corresponding values for the 2001 and 2024 scenarios were 78 mm and 87 mm, respectively. The total number of flooding events with a runoff value above 10 mm was simulated to be 88 for the 1986 land use scenario while the number for the 2001 and 2024 scenarios were 100 and 106, respectively. The number of flooding events exceeding 20 mm for 1986 scenario was 25, increased to 30 and 39 for land use scenarios of 2001 and 2024. Results show that urban expansion is a major driving force in flood generation and the projected warming and drying will not alleviate this emerging hazard. The present study highlights that urban expansion has a more significant impact on flood intensity and frequency than decreasing precipitation and rising temperatures. The study emphasizes the urgent need to integrate urban hydrology and geomorphology into land-use planning policies. The flood related information presented in this investigation is quite operational to assist in mitigating potential flood damages and future land use planning for Amman City and other urban areas in Jordan and the nearby region.

1. Introduction

Rapid urban expansion has deleterious consequences on many environmental issues such as air quality, energy consumption, and thermal comfort (e.g., Chung et al., 2011; Jahan et al., 2021; Oroud, 2022). Of particular importance is flooding, which poses significant challenges to cities worldwide, particularly in third-world countries due to a lack of adequate infrastructure and poor zoning criteria. Urban areas are prone to extensive flooding events due to the widespread impermeable surfaces which impede the absorption and retention of rainwater (Guo et al., 2021; Agonafir et al., 2023). Population growth causes inward and outward urban expansion. Inward growth fills the void spaces, causing a substantial increase of the impermeable surfaces while the outward expansion adds additional impervious landscapes to the total area contributing to flooding events.

Urban landscape has numerous negative effects on the hydrological cycle including increasing surface runoff, decreasing infiltration, and degrading water quality (e.g., Miller and Hutchins, 2017; Odeh et al., 2022). Recurrent flooding in Amman City has become ubiquitous during the rainy season in recent years. The rapid population growth, poor zoning measures, and the topography of the city go hand in hand in exacerbating the recurrence of this damaging natural hazard. Significant property losses and human casualties have been increasing in the city in recent years. A major flooding catalyst has been the substantial expansion of the impermeable urban fabrics over the steep topography during the past four decades, resulting from the rapid population growth. The population of Amman increased from ~0.8 million people in 1986 to more than 2.25 million people in 2024. The risk of flooding events is further intensified by the rugged topography and poor urban planning. Significant parts of the city are situated along the wadies, draining higher portions of the city. Improper zoning measures contributed significantly to this damaging hazard. Planners did not pay attention to the hydrology of the city prior to zoning new lands into urban land use over the higher portions of the city which caused water to significantly flood to the downtown area.

* Corresponding author e-mail: ioroud@mutah.edu.jo

In recent years, the southeastern Mediterranean witnessed aridification and warming trends , precipitation declined, and temperature showed a significant increase. This aridification and warming trends are expected to influence flood hazard in the study area provided that the intensity of precipitation did not witness any alterations.

Numerous studies were conducted to assess flooding in Amman City and nearby areas (Alhasanat, 2014; Oroud, 2015a, Oroud, 2015b; Engicon, 2019; Gharaibeh et al., 2019; Tabari et al., 2020; Al Azzam and Al Kuisi, 2021; Oroud, 2024). For instance, Ecogen (2019) reported that the intensity of precipitation that fell on the 28 of February 2019 did not justify the massive flooding in downtown Amman and attributed the flood disaster to an inadequate municipal drainage network. Other studies focused on the effect of climate change on individual and community response to flood disasters (Al Saodi et al., 2023; Gammoh et al., 2023). The relative influence of land use changes and the recent aridification-warming trends on flooding have not been addressed in earlier studies, and thus the objective of the present study is to examine the effect of land use changes and recent climate change on flooding events within the catchment area draining the city of Amman using a spatially distributed hydrological model, remote sensing data and GIS tools. The model is run on a daily timestep with a spatial resolution of 250 m to capture the fine spatial details caused by the large variations in topography and land cover. The hydrological model was run for three land use scenarios: 1986, 2001, and 2024. This study will examine the effects of urban expansion and climate change on the frequency and magnitude of flooding events in the study area.

2. Study Area

Amman City is located in central Jordan and represents the largest urban center in the country (Figure 1). The city was a very small town in the beginning of the 20th century, which was confined to a strip of low land adjacent to a creek draining the nearby rugged terrains. The small town expanded from the low-lying areas to the nearby rugged mountainous terrains in a rather random manner. The downtown area, which occupies the low-lying areas and the site of vibrant commercial activities, is situated within the confluence of the water courses draining the higher parts of the city.

The city witnessed a rapid population growth due to the recurrent influx of refugees and immigration from rural areas. The population of the city increased from ~90 thousand people in 1950 to more than ~2.25 million people in 2024. In other words, the population of the city increased by about 24 folds within the past 75 years. Following this population explosion, the city size expanded by about 20 times between 1950 and 2003 (Oroud and Al-Rousan, 2004) and by more than 70% between 2003 and 2015 (Al-Kofahi et al., 2018). Figure 2 shows the population growth of the city of Amman between 1950 and 2024.
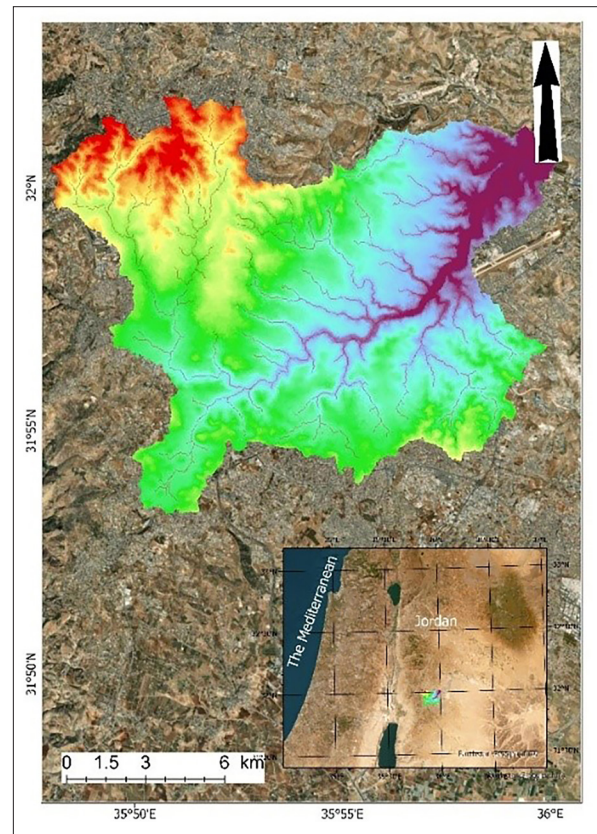
Figure 1. Location of the study area
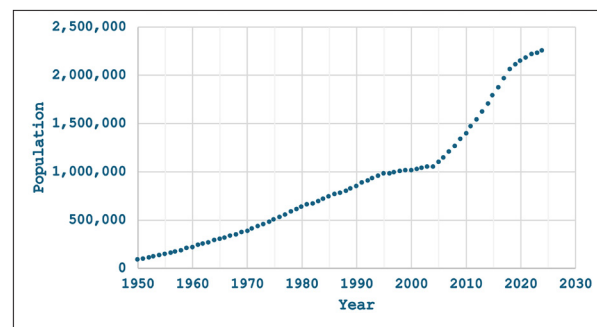
Figure 2. Population growth of Amman city during the period 1950 through 2024.

Data Source: United Nations - World Population Prospects: https://www. macrotrends.net/global-metrics/cities/21700/amman/population - Amman, Jordan.

3. Data and Method of Investigation

3.1 Meteorological Data

Daily data on the precipitation of three hydrometeorological stations was obtained from several sources including the Department of Meteorology, the Ministry of Water and Irrigation and the Ministry of Agriculture, Jordan. The daily data covers the period from 1985 through 2021. Daily data on precipitation for the three stations was cross-correlated to ensure record consistency and accuracy. Maximum and minimum air temperatures were obtained from a station within the city operated by the Department of Meteorology, Jordan.

3.2 Topography, Soil and Land Cover

The topography of the city was generated using a digital elevation model (DEM), downloaded from the Shuttle Topographic Radar Mission (STRM) from the USGS site (http://earthexplorer.usgs.gov). The DEM image, which has a spatial resolution of 30 m, was used within a GIS environment to delineate the watershed, identify the elevation of each resolution grid, and generate the various raster layers needed in the analysis of flooding and flow accumulation. The watershed, draining the city, has steep gradients with an elevation ranging from ~650 m to more than 1100 m above mean sea level. This steep topography gradient reflects the rugged nature of the city. A soil shapefile was obtained from the Ministry of Agriculture, Jordan, where each soil type was classified based on its texture (Hunting Technical Report, 1993).

The land cover for the study area was derived from Landsat images downloaded for 1986, 2001, and 2024. The three images were downloaded in April and May to identify land cover patterns correctly because arid and semiarid lands tend to give a spectral signature similar to urban landscapes during the dry season (Oroud and Balling, 2021). Landsat 5 and 7 have an 8-bit radiometric resolution, 0-255 dynamic range, while Landsat 9 has a 14-bit radiometric resolution, 0-16383 dynamic range (Table 1). This means that Landsat 9 OLI-2 has a much higher radiometric resolution, and, thus, it is capable of discerning subtle land surface tones compared to the earlier satellites images. The visible and near-infrared bands were stacked and pan-sharpened using band 8 for Landsat 7 and 9 to enhance their spatial resolution. The three images were classified using the Support Vector Machine (SVM) embedded in Arc GIS Pro (see also Oroud and Balling, 2021; Oroud, 2023).. The accuracy of the classification was checked for the image of 2024 against high-resolution Google images with a Kappa value of 92%.

Table 1. The spectral and radiometric properties of the three Landsat satellites used in this investigation.

Landsat	Date	Number of bands	Radiometric resolution	Spatial resolution
Landsat 5 TM	4-5-1986	7	8-bit	30 m
Landsat 7 ETM+	24-5-2001	8	8-bit	30 m
Landsat 9 OLI-2	05-4-2024	11	14-bit delivered to users as 16-bit	30 m

3.3. GIS tools

The GIS tools were implemented to generate watersheds and obtain the x, y coordinates and elevation values for each resolution cell. Land-cover type, soil classes and slope were overlain in a GIS environment to generate a curve number across the study area during the three land use scenarios—1986, 2001, and 2024. The curve number generated for each scenario was used in the hydrological model to calculate flooding frequency, magnitude, and its spatial distribution across the study area. The GIS tools were also used to extract the flow accumulation which can be used for operational purposes to examine flood volume for sub-watersheds.

3.4. Data Interpolation

The introduction of GIS at the end of the previous century has revolutionized data interpolation, and, thus, large spatial extents could easily be interpolated objectively and with a high degree of accuracy given the availability of a sufficient number of measuring points. The problem of direct GIS interpolation schemes can become problematic if weather-measuring stations are sparingly distributed over rugged terrains (e.g., Jeffrey et al., 2001; Apaydin et al., 2004), leading to large errors. A more rigorous procedure to interpolate meteorological data would be to take into account vertical and horizontal gradients of the specified element across the landscape (e.g., Schoener, 2010; Emmendorfer and Dimuro, 2020):

$$\delta_{i,k} = \sqrt{(x_i - x_j)^2 + (y_i - y_j)^2} \tag{1}$$

where $\delta_{i,k}$ is the Euclidean distance (m) between station I and the intended grid cell, and the x and y are the easting and northing coordinates (m). A climatological element at a grid, e.g., precipitation ($x(x_k, y_k, z_k)$ or any other climatological element like temperature, can be derived explicitly using, for example, the IDW (Emmendorfer and Dimuro, 2020; Oroud, 2022):

$$x(x_k, y_k, z_k) = \frac{\sum_{i=1}^{j}(x_i + \Gamma(z_i - z(k))/\delta(i,k)^2}{\sum_{i=1}^{j}\frac{1}{\delta(i,k)^2}} \tag{2}$$

where x_k is the easting (m), y_k is the northing (m) and z_k is the elevation of the grid; x_i is the meteorological element at station I, Γ is the environmental gradient/lapse rate (e.g., mm m^{-1}), z_i is the elevation of station I, z(k) is the elevation of the grid, and $\delta(I,K)$ is the Euclidean distance between station I and the intended cell. Precipitation for each grid was interpolated using the Inverse Weighing Distance using the three meteorological stations after accounting for grid elevation. The interpolation of air temperature is easier because this element depends primarily on the elevation difference between the grid and the measuring station.

3.5 The Hydrological Module

For modeling purposes, the study area was subdivided into discrete cells, each of which is 250 m side length. Each cell has its X and Y coordinates along with its unique CSN value. The Soil Conservation Service Curve Number (SCS-CN) scheme is widely implemented to characterize flooding over urban areas (e.g., Ponce and Hawkins, 1996; Dingman, 2002; Kannan et al., 2008; Jahan et al., 2021; Oroud, 2024). The SCS method implements the curve number to assess runoff response as a function of soil type, land cover, the state of landcover and topography (Borga et al., 2007; Ries et al., 2017).

The maximum potential soil moisture retention capacity (S) is derived based on the Curve Number of each resolution cell (Ponce and Hawkins, 1996):

$$S(j) = 254\left(\frac{100}{CN(j)} - 1\right) \tag{3}$$

where S(j) is the moisture potential retention capacity, and CN is the curve number of the pixel. The S(j) of soil is adjusted between the dry soil condition (CN1) and the wet conditions (CN3) as determined from the antecedent soil moisture of each resolution cell (Ponce and Hawkins, 1996),

$$CN1 = \frac{CN}{2.28 - .01281CN} \tag{4}$$

$$CN3 = \frac{CN}{0.427 + 0.00573CN} \tag{5}$$

The CN value for a resolution cell at a given time step is as follows:

$$CN = CN1 + \frac{\mu S i^{t-1}}{S_{max}} \tag{6}$$

where S_{max} is the soil moisture retention capacity at CN1; Si^{t-1} is soil moisture retention of a resolution cell at the previous timestep (previous day), μ is determined by Ponce and Hawkins, 1996:

$$\mu = CN3 - CN1 \tag{7}$$

The curve number is adjusted for slope as suggested by Ajmal et al. (2023):

$$CN = \frac{322.79 + 15.63\alpha}{323.52 + \alpha} \tag{8}$$

where α is the slope in percentage.

Runoff from a given grid occurs when daily precipitation exceeds its moisture potential retention (e.g., Viola et al., 2017):

$$\left\{ \begin{matrix} Ro = \frac{(P - 0.2S)^2}{P + 0.8S}, P > 0.2S \\ Ro = 0, P \leq 0.2S \end{matrix} \right\} \tag{9}$$

4. Evaporation Calculation

For the non-steady state of transient modeling, there must be tracking of surface moisture as antecedent moisture has a significant impact on actual evapotranspiration, surface runoff and groundwater recharge. The soil water change is established by using the water budget at the surface, expressed as (e.g., Viola et al., 2017; Small et al. 2018):

$$\frac{\delta S}{\delta t} = P - A_T - R_O - D_p \tag{10}$$

where the first term on the left is soil moisture change with respect to time, P, A_T, R_O, and D_p, are precipitation, actual evapotranspiration, surface runoff, and deep percolation, respectively.

Actual evapotranspiration is determined by potential evapotranspiration, soil water content, and subsurface hydraulic properties (Dingman 2002; Allen et al., 2007). Actual evaporation is calculated as a function of potential evaporation and soil moisture content within a resolution pixel. In this study, potential evapotranspiration (PE) is calculated using the following form (Hargreaves and Allen 2003):

$$PE = 0.0023 R_g \left(17.8 + \bar{T} \right) \sqrt{\Delta T} \tag{11}$$

where PE is potential evapotranspiration (mm/day), R_g is daily global radiation in mm equivalent units, is the average daily temperature (OC), and ΔT is the diurnal temperature range, the maximum minus the minimum temperature.

Global radiation is parameterized by Hargreaves and Samni (1982):

$$Rg = 0.408 S_{ext} \tag{12}$$

where S_{ext} is the extraterrestrial daily solar radiation as determined by latitude and declination of the sun (Iqbal, 1983):

$$S_{ext} = S_C R(\omega \sin \varphi \sin \delta + \cos \varphi \cos \delta \sin \omega) \tag{13}$$

where SC is daily solar radiation constant at the mean earth- sun distance, R, Φ, δ, and ω are the sun-earth distance ratio (-), latitude, declination of the sun, and daylength. The simulated daily extraterrestrial radiation in the study area varies from ~18 MJ m^{-2} day^{-1} at the end of December to ~ 42 MJ m^{-2}day^{-1} in June. It is important to note that in the Mediterranean region precipitation and evapotranspiration are out of phase, and the major factor influencing water balance and flooding is precipitation (Unissa et al., 2023; Oroud, 2024). Furthermore, the long dry and hot summer season deletes the past memory of subsurface moisture storage, and, thus, a hydrological year can be modeled independently from previous years with very little, if any, loss of accuracy (e.g., Viola et al., 2017).

In this study, the soil profile is divided into two compartments, a top thin one with a moisture holding capacity of 15% of the total soil profile capacity, and a deep layer holding 85% of the total soil moisture. This procedure was adopted successfully by numerous researchers and gave excellent results (e.g., Palmer, 1965; Crooks and Naden, 2007). Actual evapotranspiration is assumed to be equal to the potential value (PE) when precipitation equals or exceeds P but decreases nonlinearly as soil moisture drops (e.g., Farmer et al., 2003; Liu and Smedt 2004; Enrique and Alfonso, 2010):

$$AE = PE, P \geq PE$$

$$AE = (P_E - A_{E1}) \left(\frac{\theta - \theta_w}{\theta_s - \theta_w} \right)^{\sigma}, \quad AE = AE_1 + AE_2 \tag{14}$$

where A_{E2} is evapotranspiration from the second layer, AE1 is evaporation from the top layer, θ_w is soil moisture at the wilting point, and σ is an exponent larger than unity (e.g., Liu and Smedt 2004; Crooks and Naden 2007).

5. Model Verification

There are no actual measurements to establish the performance of the present model, but we used two different procedures to establish the adequacy of the model output. The present model results were tested against the simulation results of other hydrological models and the chloride mass balance in a similar environment. The present model results are commensurate with the chloride mass balance and the simulation results of other hydrological models (see Oroud, 2024). Because of the lack of direct flood observations, we resorted to archived newspapers and social media data which reported the extent of flood damage and pictured the flood magnitude. Thus, we used the archived flooding events for Amman City for the period 2010 through 2021, as reported in the local newspapers and social media. Archived flooding events were compared to those generated by the model using the 2024 land use scenario. It is well understood that flooding is closely linked to precipitation intensity—e.g.,

hourly, 3 hours, and 6 hours, which cannot be revealed by the model as it uses a daily timestep. Yet, newspaper reports would give a good indication of flooding magnitude and thus can be used to "gauge", at least qualitatively, the simulation results. Table 2 shows the dates along with precipitation and flooding magnitudes exceeding 20 mm along with the reported flooding events in the newspapers' archives for the period 2010-2021.

Table 2. The dates along with precipitation and flooding events exceeding 20 mm/day for the period 2010-2021 and flooding events as reported in the archives of newspapers.

Date	Precipitation (mm/day)	Flood magnitude (mm)	Newspapers reports
18-1-2010	51.12	28.38	No flooding reports
26-2-2010	51.92	33.18	Heavy flooding in downtown
28-2-2010	45.21	28.17	No flooding reports
4-2-2011	38.1	21.09	No flooding reports
17-2-2011	41.19	22.15	No flooding reports
29-2-2012	43.34	25.04	No flooding reports
1-3-2012	55.68	25.76	No flooding reports
7-1-2013	75.4	53.4	Heavy flooding reports
8-1-2013	54.88	37.21	Heavy flooding reports
11-12-2013	55	34.04	Heavy flooding reports
26-11-2014	37.57	20.04	No flooding reports
18-2-2015	46.55	21.19	No flooding reports
8-1-2016	37.7	21.07	No flooding reports
5-1-2018	43.74	25.16	Heavy flooding reports
18-1-2018	37.43	20.78	Heavy flooding reports
27-2-2019	42.13	24.17	Heavy flooding reports
28-2-2019	58.23	40.68	Heavy flooding reports
26-12-2019	83.32	54.03	Heavy flooding reports
8-1-2020	47.5	30.27	Heavy flooding reports

It is clear that whenever flooding exceeded 30 mm/day, massive flooding was reported. Archived results show good agreement with simulation results. The model failed to identify a major flooding event reported on 5-11-2015. This flooding event was a result of an intense localized thunderstorm that lasted for 40 minutes, and the reported precipitation across the catchment was 13 mm. The overall agreement between simulated and archived flooding events provides further support to the adequacy of the model results.

6. Results

6.1. Urban Expansion

Figure 3 shows the city size in 1986, 2001, and 2024 as obtained from Land-sat images. There has been a large urban expansion during the past four decades which reflected the rapid population growth of the city. Urban areas within the catchment area increased from ~83 km² in 1986 to ~137 km² in 2024, an increase of about 64%. On the other hand, cultivated and forest areas decreased from 68 km² and 28 km² in 1986 to ~32 km² and ~11 km² in 2024. This is a substantial land cover change during the past 40 years. The transformation of natural landscapes into highly impermeable urban fabrics is expected to heighten flood risk and reduce the concentration time of flood peaks.

This land use change reflected the very rapid population growth of the City of Amman. The number of inhabitants of the city increased from ~800 thousand in 1986 to 2.25 million people in 2024. Figure 4 shows the distribution of land use in 1986 and 2024.
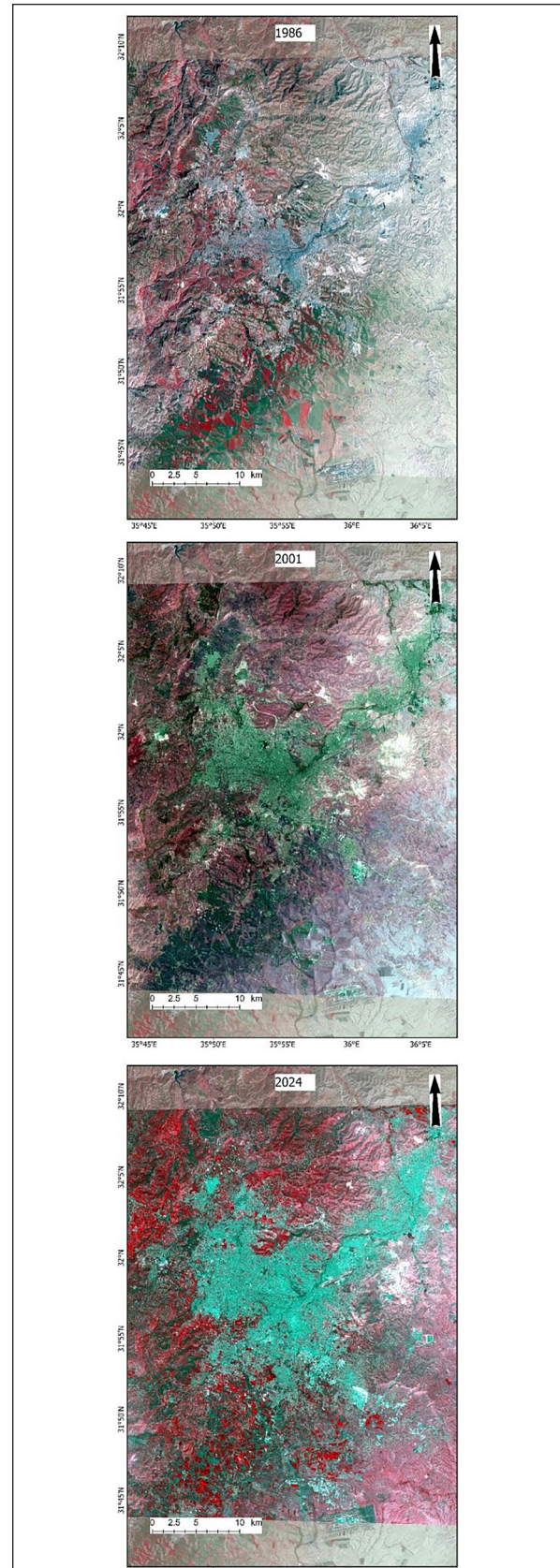
Figure 3. Urban expansion of the city of Amman as revealed by three Landsat images taken in 1986, 2001, and 2024
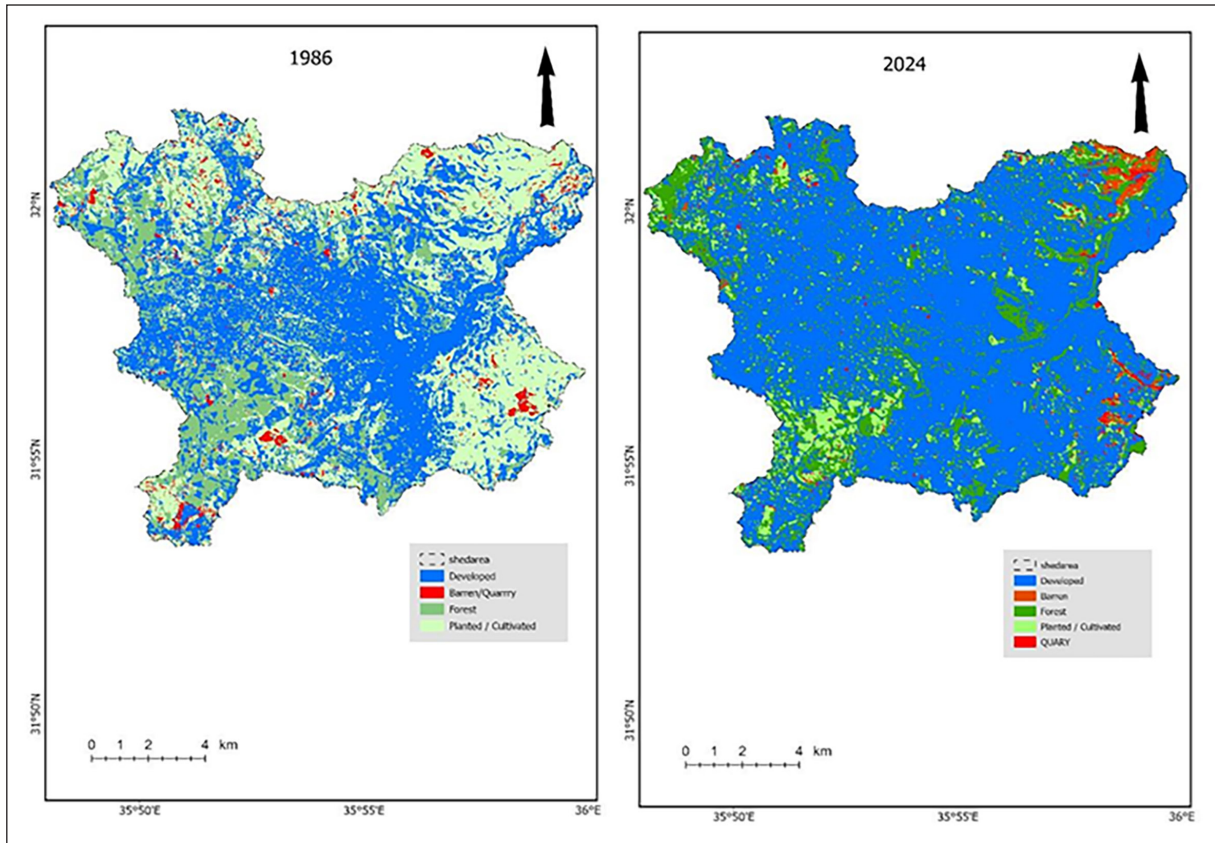
Figure 4. The extent and spatial distribution of land use in 1986 and 2024.

6.2. Spatial distribution of precipitation

There is a steep precipitation gradient across the watershed which typifies the Eastern Mediterranean environment. Precipitation follows closely the elevation contour lines. Figure 5, which is generated by the model, shows the average annual precipitation distribution across the catchment; it ranges from a minimum of ~200 mm/year in low laying areas to more than 420 mm/year in the northwestern parts of the catchment where elevation reaches 1100 m.

6.3 Precipitation Events

Precipitation in the Eastern Mediterranean falls from October through May. More than 75% of precipitation occurs in the coldest months, December through February. Yet, large precipitation events also occur in the transitional seasons—Fall and Spring—mainly due to dynamic atmospheric static instability caused by upper air cold troughs advancing from the northwest, associated with low level moist warm air and penetrating along the Red Sea Trough (e.g., Oroud, 2018; Hochman et al., 2022). Figure 6 shows the frequency of precipitation categorized according to its daily amount. There were 1700 daily precipitation events (P>0 mm) during the 37-year study period, of which 273 events exceeded 10 mm, and 113 events exceeded 20 mm/day.

Figure 5. The spatial distribution of precipitation (mm/year) along with the elevation contour lines (meters above mean sea level)
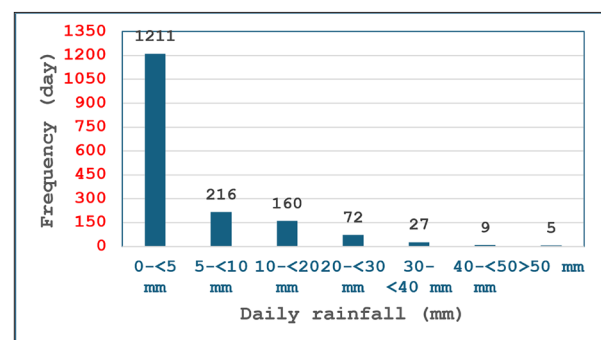
Figure 6. The frequency of precipitation as categorized according to its daily amount

Annual precipitation has decreased slightly during the past 37 years. Still, it is not statistically significant while the minimum and maximum temperatures exhibited significant increasing trends which are important at the 95% level (see Figure 7). The average maximum air temperature in the study area was 23.22 °C during 1985-2005, while its corresponding value for the second period, 2006 -2021, was 24.22 °C. Likewise, the average minimum temperature for the first period was 12.04 °C, while it was 13.14 °CC in the second period. This increasing trend is linked to global warming and urban expansion. A temperature increase is likely to reduce flooding and groundwater recharge due to the increased water loss via evaporation provided that the intensity of precipitation did not experience any change. Examination of daily precipitation data did not reveal any statistically significant changes in the intensity of precipitation during the study period. Thus, based on climate alone, there should be a reduction in runoff because of the increased air temperature.
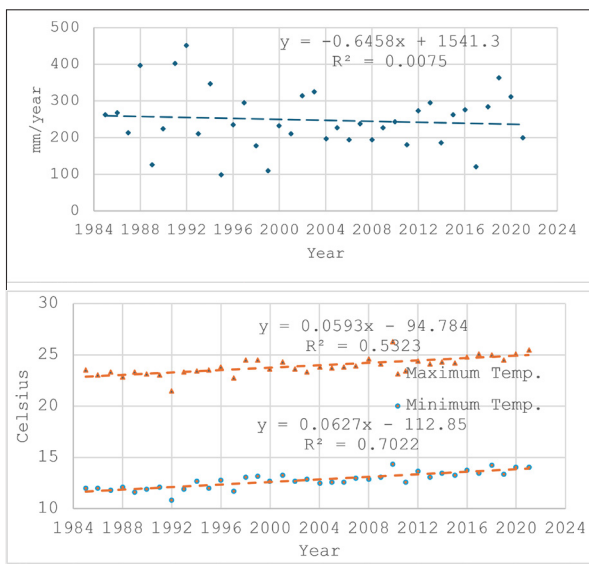
Figure 7. Annual precipitation and minimum and maximum temperature trends during the period 1985 through 2021

6.4 Runoff and Flooding Events

The significant changes in land use during the past 40 years have caused a large change in the curve number. For instance, the curve number as derived from the Landsat images was 86.0 for 1986 land use scenario, increased to 87.7 and 89.7 for land use scenarios of 2001 and 2024. Although the change in the curve number is relatively small, it is important to note that the curve number is quite high to start with, and, thus, small departures in the CN are expected to amplify runoff events significantly following urbanization expansion. Simulation results show that the average annual surface runoff for 1986 land use scenario was ~71 mm which represents ~22% of average annual precipitation while the corresponding values for 2001 and 2024 land use scenarios were 78 mm and 87 mm, respectively. The increased runoff came mainly at the expense of actual evapotranspiration. For instance, actual evapotranspiration for the 1986 scenario was 198 mm while it is 192 mm and 178 mm for 2001 and 2024 land use scenarios.

Figure 8 shows the link between daily precipitation and daily runoff for the 1986 and 2024 land use scenarios. It is clear that runoff link to precipitation exhibits a steeper response for the 2024 land use scenario as demonstrated by visual inspection and the coefficients of the regression line. Runoff tends to start, in general when precipitation exceeds 10 mm for land use scenario of 2024 but has a higher precipitation threshold for 1986 land use scenario.
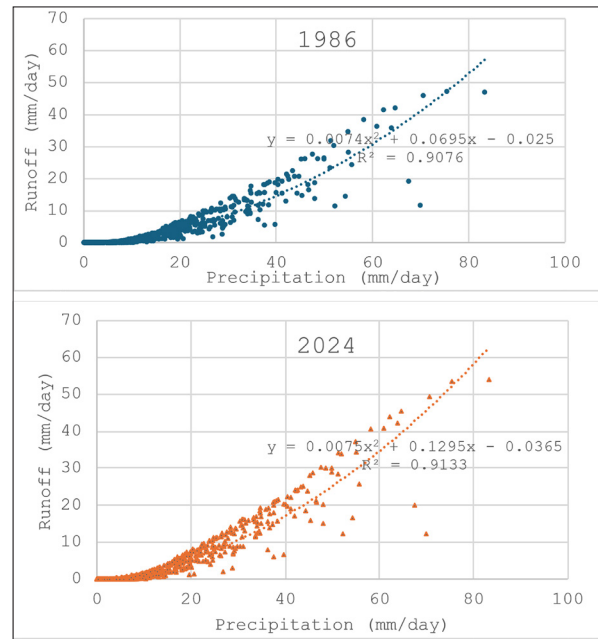
Figure 8. The link between daily precipitation and daily runoff for the 1986 and 2024 land use scenarios. Notice that the curve is steeper for land use scenario of 2024 as revealed by the regression coefficients.

A more dramatic effect of urbanization is quite distinct when examining the frequency of flooding events according to their magnitudes. Table 3 shows the runoff events categorized based on their magnitude under the three land use scenarios using the same daily precipitation and temperature records. The total number of flooding events for the three scenarios were not very different from each other, with a value ranging from 760 to 706. The picture becomes very different when comparing large flooding events among the three scenarios. For instance, the number of flooding events (runoff 10 mm) is 88 for the 1986 land use scenario, increased to 100 and 106 for 2001 and 2024 land use scenarios. The departure becomes far more distinct when comparing very large flooding events. For instance, the number of flooding events of 20 mm/day is 25 for the 1986 land use scenario while it is 39 for land use scenario of 2024, with a 56% increase. The land use scenario of 1986 did not show any flooding events in excess of 50 mm/day. Results demonstrated that the frequency of large flooding events has increased substantially following the spread of urbanization. This increase clearly demonstrates that urbanization has a significant impact on flooding in Amman despite the buffering effect brought about by precipitation reduction and air temperature rise.

Table 3. Number of runoff events categorized based on magnitude for the city of Amman as influenced by land use scenarios of 1986, 2001, and 2024. The simulation for each scenario was run from 1985 through 2021.

Runoff magnitude (mm/day)	Number of runoff events for each land use scenario			
	1986	2001	2024	% change between 2024 and 1986
>=0	759	760	766	1%
>=10	88	100	106	20%
>=20	25	30	39	56%
>=30	11	12	15	36%
>=40	5	5	8	60%
>=50	0	2	2	----

An important point is the effect of land use changes on the simulated spatial distribution of floodwater across the catchment. Figure 9 shows the average annual distribution of runoff across the catchment in 1986 and 2024. It is clear that a significant increase in runoff potential is observed for land use of 2024 compared to 1986. The alteration from agricultural and forest lands to urbanization has significantly reduced the surface capacity to absorb and retain precipitation, leading to higher runoff potential. The effect of slope on flood generation is taken into account via Eqn. 8, which implies a larger increase in the curve number as slope gradient increases. Furthermore, the combination of impermeable surfaces along with steep slopes reduces the concentration time for flood peaks.
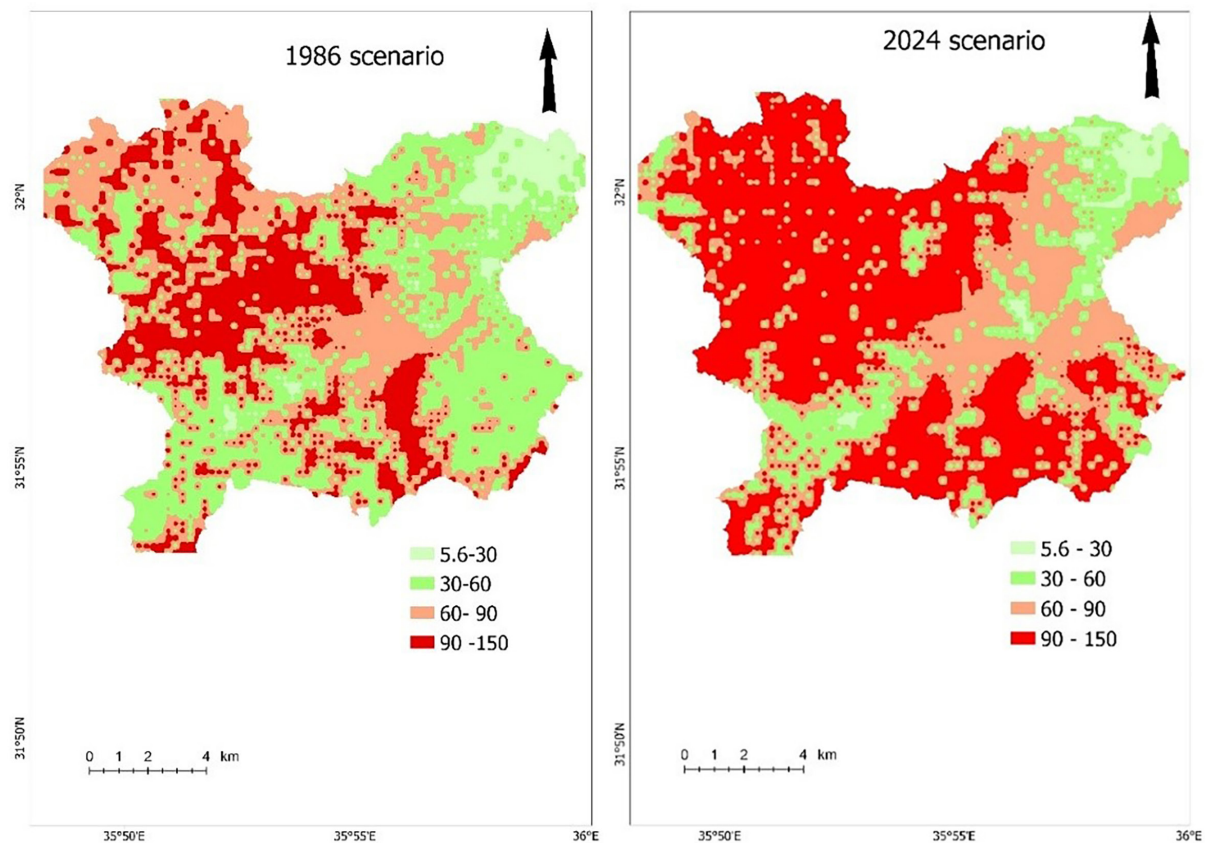
Figure 9. The average annual distribution of runoff (mm/year) across the catchment area in 1986 and 2024

6.5 Climate Change Versus Urbanization

To examine the effect of land use changes compared to climate change impacts, we subdivided the period into two parts; one extends from 1986 through 2005, and the other extends from 2006 through 2021. It is assumed that the land use in 1986 represented the first period while the second period was assumed to be represented by the land use in 2024. Calculations show that the average annual potential evapotranspiration and precipitation during the first period were 1323 mm and 340 mm while the corresponding values for the second period were 1359 mm and 323 mm, respectively. Clearly, a trend of aridification and warming is observed during the second period. Based on climate records alone, we should expect more surface runoff during the first period. Figure 10 shows that the number of flooding events 20 mm/day during the first period was 10 while in the second period, which represents land use of 2024, recorded 21 events, more than 100% increase in flooding events.
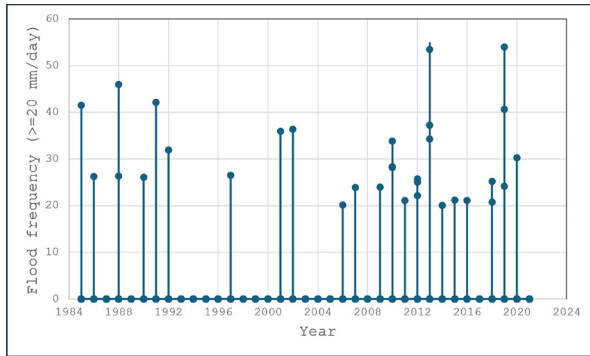
Figure 10. The number of flooding events over 20 mm/day. The land use scenario of 1986 represents the period 1986 through 2005 while the land use scenario of 2024 represents the period 2006 through 2021. Each dot in the figure represents a flooding event >= 20 mm/day.

The large increase in flooding events during the second period was only due to land use changes . The frequency of major precipitation events did not show any difference between the two periods. For instance, the number of daily precipitation events over 20 mm in the first period was 57, while it was 56 in the second period. Likewise, the number of precipitation events over 30 mm was 21 events in the first period and 20 events in the second period. This means that the significant increase in large flooding events simulated in the second period was due to land use changes. Thus, the buffering effect, brought about by aridification and warming in the second period, did not have any effect in reducing large flooding events in the study area despite the warmer and drier conditions experienced in the second period.

7. Discussion

The natural setting of Amman City, being highly urbanized and built over rugged terrain, increases the risk of flooding and poses serious threats to infrastructure and human lives, particularly in the downtown area as it represents a confluence of the various tributaries draining the upper parts of the watershed. Figure 11 can be employed for operational purposes to identify the volume of flow, peak flow and time of concentration given a specific precipitation amount. Digital elevation data can be used to identify the sub-watersheds using GIS tools, and thus the hydrological model can be implemented to estimate the volume and timing of flooding expected near the outlet of each sub-watershed.

The expected flood volume for a given tributary crossing the downtown area can be calculated using the runoff results obtained from the hydrological model along with the accumulation raster derived from the digital elevation model, using the following form:

$$QA = \sum_i^n Ri \, \Delta A \qquad (15)$$

where QA is runoff volume, Ri is the runoff (mm) potential, and ΔA is the contributing area (m²). For instance, if Ri is 20 mm and the total area contributing to the sub watershed is one km², then the total volume of flood is expected to be ~20 thousand m3. Because of the rugged terrains and impermeable surfaces, the time of concentration for storms is relatively short, in the order of less than one or two hours, which leaves very little time to take precautionary measures. For operational purposes, each tributary can be examined separately to identify the level of danger it poses.
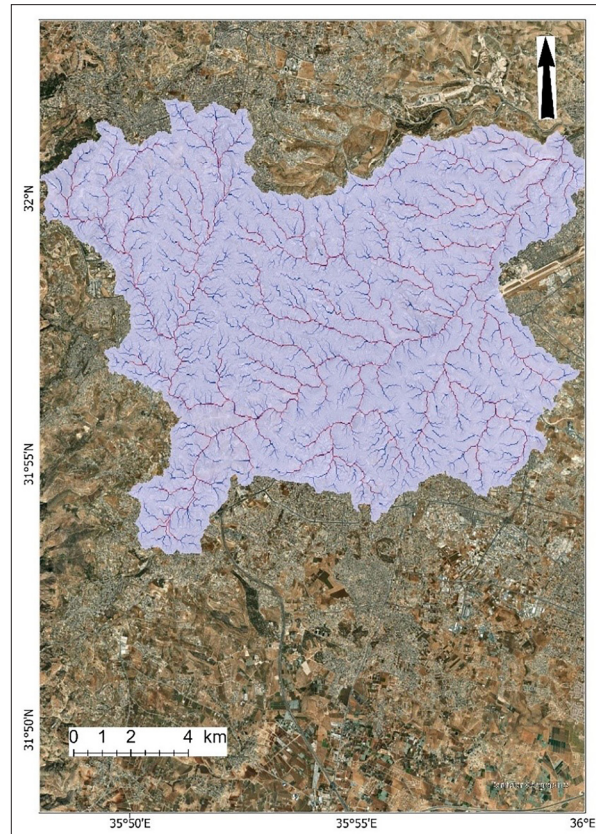
Figure 11. The sub watersheds within the study area. Note that the various drainage network confluence in the downtown area.

Flood hazards further worsen when examining the road and drainage networks. Figure 12 shows the various tributaries superimposed on the city street network. The street network in the downtown area- Al-Madina- is aligned along major tributaries draining huge, urbanized sections within the watershed. This means that large volumes of flood water would inundate the downtown area and major roads, leading to human casualties, significant monetary losses, traffic accidents and serious disruption to traffic flow (see Figure 13). Thus, increased urbanization has significantly increased the probability of large flooding events in recent years as demonstrated by the simulation results and the reported floods. The capacity of natural surface to hold moisture is much higher than those for urban landscapes. As CN increases as in the case for urban fabrics, a large portion of precipitation is converted to surface runoff. These results are commensurate with results presented by other investigators such that the hydrological changes of urbanization will increase the flood peaks and decrease the concentration times (e.g., Huong, and Pathirana,(2013, Miller and Hutchins, 2017) .

It is clear that urbanization is a significant factor in causing major flooding events in recent years. Presented results are consistent with observations obtained elsewhere. For instance, Birhanu et al. (2016) found that urbanization in Adiss Ababa in Ethiopia increase runoff by 25%. Furthermore, Bian et al. (2017) observed a 60% runoff increase in a river basin in southern China, indicating that urbanization was responsible for 59% of this increase while climate change was responsible for only 1% .
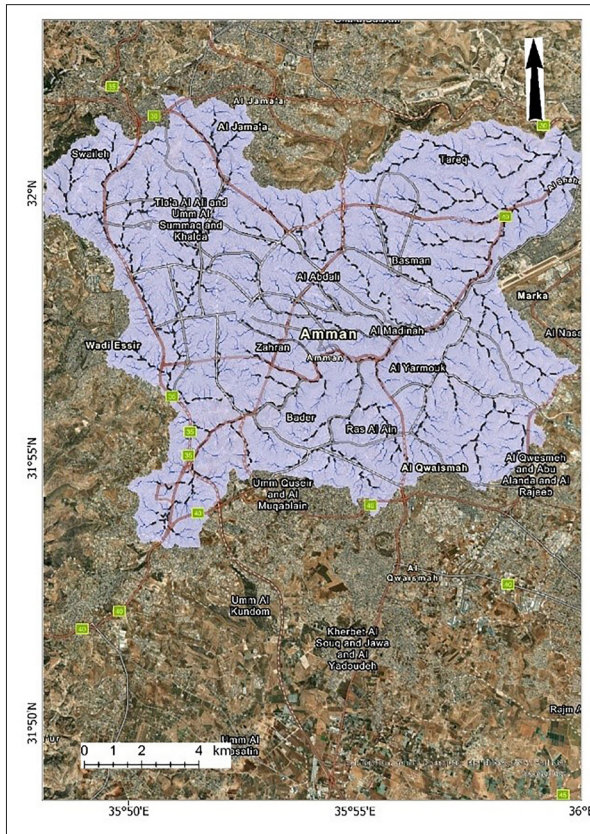
Figure 12. The various tributaries superimposed on the city road network.

Uncontrolled urbanization degrades water quality, reduces agricultural and forest lands, and increases the frequency and volume of surface runoff because of the increased imperviousness. An important urban development plan to cut down on the flooding risk, particularly for cities situated over rugged terrains, would be to study the geomorphology and watershed hydrology of the planned area prior to zoning an area for urban land use purposes. For instance, upper parts of a catchment area contributing to flooding should be zoned as agricultural/forest or parklands to eliminate, or, at least, reduce the risk of large flooding events. The effect of climate change on the frequency and magnitude of flooding does not seem to be of any importance in alleviating the flood hazard in the study area.

Figure 13. A typical flooding event inundating Downtown Amman City. This photo was taken on 28/2/2019.

8. Conclusion

Impervious surfaces and buildup land are more vulnerable to flooding than natural landscapes. The increased probability of flooding poses serious risk factors to human lives, human health, property, traffic flow and accidents. Sustainable urban planning, expansion of green infrastructure, proper zoning, and improved drainage network play pivotal roles in reducing flood vulnerabilities. The increased precipitation intensity projected by global warming will more likely exacerbate severe flooding events in the study area in the future unless more adequate engineering measures are adopted to mitigate this natural hazard. Strategies such as stormwater drainage networks play a pivotal role in mitigating the effect of flooding events in Amman. The poor zoning measures contributed significantly to the high risk of flooding because the higher areas, which were supposed to be left as agricultural land or implanted with forests, increased the probability of large flooding events. The improper and uncontrolled urban expansion on the agricultural and natural landscape such as forests has substantially increased the risk of flooding in Amman City.

Results demonstrated clearly that urban expansion surpassed the aridification and warming trend observed in the study area. The number of large flooding events has experienced a large increase in recent years despite the fact that precipitation declined, and air temperature rose substantially. There is no magic solution to the dilemma of the repeated flooding and inundations in downtown Amman City due to the limitations imposed by the topography of the city and the spatial distribution of roads and commercial properties. Although the presented model depicts flooding events very adequately, the availability of precipitation data at hourly timesteps would more likely mimic more accurately the flooding events spatially and temporally.

Measurements of precipitation and flood events using real- time data are crucial for future modeling purposes and urban planning. It is highly advisable to install a dense precipitation network across the flood- contributing areas within Amman City to monitor precipitation amount and intensity. This precipitation network should be remotely monitored through various relevant agencies such the Civil Defense Department and Amman Municipality to take precautionary measures ahead of flooding events to mitigate the adverse consequences.

Proper modeling techniques have the capability to provide adequate projection of flooding events at the watershed and sub watershed scales, thereby guiding decision-makers to take proper measures to mitigate flooding events and protect lives, infrastructure, and the economy. It is imperative to study the geomorphology and hydrology of an area prior to zoning it for urban development to avoid the consequences of costly flooding events. Findings of this study should prompt decision makers for setting environmental and urban expansion legislations to control flooding and also for managing the urban water environment and identifying knowledge gaps that limit effective management interventions.

References

Agonafir, C., Lakhankar, T., Khanbilvardi, R., Krakauer, N., Radell, D., Devineni, N (2023) A review of recent advances in urban flood research, Water Security, 19, https://doi.org/10.1016/j.wasec.2023.100141.

Alhasanat, H. (2014) Flash flood assessment for Wadi Mousa City-Jordan, Procedia Economics and Finance, 18, 675- 683, doi:10.1016/S2212-5671(14)00990-3

Ajmal, M., Waseem, M., Jehanzaib, M., Kim, T (2023) Development and testing of updated curve number models for efficient runoff estimation in steep-slope watersheds, Journal of Hydrology. 617, https://doi.org/10.1016/j.jhydrol.2022.129049.

Al-Kofahi, S.D., Hammouri, N., Sawalhah, M.N. (2018) Assessment of the urban sprawl on agriculture lands of two major municipalities in Jordan using supervised classification techniques. Arab Journal of Geosciences, 11, 45, https://doi.org/10.1007/s12517-018-3398-5

Allen, R.G., Tasumi, M., Morse, A., Trezza, R., Kramber, W., Lorite, I., Robinson, C.W. (2007) Satellite-based energy balance for mapping evapotranspiration with internalized calibration (METRIC) – Applications. Journal of Irrigation and Drainage Engineering, 133–395, 406.

Al Saodi, R., Al Kuisi, M., Al Salaymeh, A. (2023) Assessing the vulnerability of flash floods to climate change in arid zones: Amman–Zarqa Basin, Jordan, Journal of Water and Climate Change, 14 (12): 4376–4403. https://doi.org/10.2166/wcc.2023.237

Al Azzam, N., Al Kuisi, M. (2021) Determination of flash floods hazards and risks for Irbid governorates using hydrological and hydraulic modelling, Jordan Journal of Earth and Environmental Sciences, 9, 81-91.

Apaydin, H., Sonmez, FK., Yildirim, YE. (2004) Spatial interpolation techniques for climate data in the GAP region in Turkey. Climate Research, 28:31–40, https://doi.org/10.3354/cr028031.

Bian, G.D., Du,J.K.. Song, M.M., Xu, Y.P., Xie, S.P., Zheng, W.L., Xu C.-Y. (2017) A procedure for quantifying runoff response to spatial and temporal changes of impervious surface in Qinhuai River basin of southeastern China, CATENA, 157, 268-278, https://doi.org/10.1016/j.catena.2017.05.023.

Birhanu D, Kim,H., Jang, C., Park, S. (2016)Flood Risk and Vulnerability of Addis Ababa City Due to Climate Change and Urbanization, Procedia Engineering,154,696-702,https://doi.org/10.1016/j.proeng.2016.07.571.

Borga, M., Boscolo P, Zanon F, Sangati, M. (2007). Hydrometeorological analysis of the 29 August 2003 flash flood in the Eastern Italian Alps. American Meteorological Society, 1049–1067. https://doi.org/10.1175/JHM593.1

Chung, E., Park, K., Lee, K. S. (2011) The relative impacts of climate change and urbanization on the hydrological response of a Korean urban watershed, Hydrological Processes, 25, 4, 544-560, doi:10.1002/hyp.7781

Liu, YB., De Smedt, F. (2004). A GIS-based hydrological model for flood prediction and watershed management (Documentation and User Manual). Department Hydrology and Hydraulic Engineering, Vrije Universiteit Brussel.

Dingman, S. L. (2002). Physical hydrology (2nd ed.). Prentice Hall.

Emmendorfer, LR., Dimuro GP. (2020) A novel formulation for inverse distance weighting from weighted linear regression. In: Krzhizhanovskaya V et al (eds) Computational Science – ICCS 2020. ICCS 2020. Lecture Notes in Computer Science, 12138. Springer, Cham. https://doi.org/10.1007/978-3-030-50417-5_43

Engicon (2019) Amman Downtown Flood on 28 Feb. 2019: Preliminary Technical Report, Prime Ministry, Amman, Jordan.

Farmer, D., Sivapalan, M., & Jothityangkoon, C. (2003). Climate, soil, and vegetation controls upon the variability of water balance in temperate and semiarid landscapes: Downward approach to water balance analysis. Water Resources Research, 39, 1035–1049. https://doi.org/10. 1029/2001WR000328

Gammoh, L., A., Dawson, T, G., Katsikopoulos,, K (2023) How flood preparedness among Jordanian citizens is influenced by self-efficacy, sense of community, experience, communication, trust and training, International Journal of Disaster Risk Reduction, https://doi.or /10.1016/j.ijdrr.2023.103585.

Gharaibeh, A. A., Zu'bi, A., Esra'a, M., Abuhassan, L. B. (2019) Amman (City of Waters); Policy, land use, and character changes, Land, 8, 12, 195, doi:10.3390/land8120195

Guo, K., Guan, M., Yu, D (2021) Urban surface water flood modelling – a comprehensive review of current models and future challenges, Hydrological Earth System Science, 25 (5) (2021) 2843–2860, https://doi.org/10.5194/hess-25-2843-2021.

Hargreaves, G. H., Allen, R. G. (2003). History and evaluation of Hargreaves evapotranspiration equation. Journal of Irrigation and Drainage Engineering, ASCE, 129(1), 53–63.

Hargreaves, G. H., Samni, Z. A. (1982). Estimation of potential evapotranspiration. Journal of Irrigation and Drain age Division, Proceedings of American Society of Civil Engineering, 108, 223–230.

Hochman, A., Marra, F., Messori, G., Pinto, J. G., Raveh-Rubin, S., Yosef, Y., and Zittis, G. (2022) Extreme weather and societal impacts in the eastern Mediterranean, Earth System Dynamics, 13, 749–777, https://doi.org/10.5194/esd-13-749-2022.

Hunting Technical Services (1993) The Soils of Jordan. Ministry of Agriculture, National Soil Map and Land Use Project, Level 1: Reconnaissance Soil Survey (Scale 1: 250,000), 3 Volumes, Amman

Huong, H. T. L., Pathirana, A. (2013) Urbanization and climate change impacts on future urban flooding in Can Tho city, Vietnam, Hydrological Earth System Science, 17, 379–394, https\\w.hydrol-earth-syst-sci.net/17/379/2013/ doi:10.5194/hess-17-379-2013

Jahan, K.; Pradhanang, S.M.; Bhuiyan, M.A.E (2021) Surface Runoff Responses to Suburban Growth: An Integration of Remote Sensing, GIS, and Curve Number. Land, 10, 452. ttps://doi.org/10.3390/land10050452

Jeffrey S, Carter J, Moodie K, Beswick A (2001) Using spatial interpolation to construct a comprehensive archive of Australian climate data. Environmental Modeling Software, 16:309–330

Kannan, N., Santhi, C., Williams, J. R., and Arnold, J. G. (2008). "Development of a continuous soil moisture accounting procedure for curve number methodology and its behavior with different evapotranspiration methods." Hydrological Processes, 22(13), 2114–2121.

Liu, YB., De Smedt, F. (2004). A GIS-based hydrological model for flood prediction and watershed management (Documentation and User Manual). Department Hydrology and Hydraulic Engineering, Vrije Universiteit Brussel.

Miller, J. D., Hutchins M. (2017) The impacts of Urbanization and climate change on urban flooding and urban water quality: A review of the evidence concerning the United Kingdom, Journal of Hydrology: Regional Studies,12,2017,345-362, https://doi.org/10.1016/j.ejrh.2017.06.006., (https://www.sciencedirect.com/science/article/pii/S2214581817300435)

Odeh, T., Mohammad, A.H., Pradhanang, S.M., Ismail, M., Rödiger, T. (2022) GIS-based analytical modeling on

evaluating impacts of urbanization in Amman water resources, Jordan. Environmental Earth Sciences, 81, 160 (2022). https://doi.org/10.1007/s12665-022-10238-7

Oroud, I. M. (2015a). Water budget assessment within a typical semiarid watershed in the Eastern Mediterranean. Environmental Processes, 06/2015; 3(2):1–15. https://doi.org/10.1007/s40710-015-0072-8.

Oroud, I. M (2015b) Water balance in a typical watershed in the Karak Plateau. Jordan Journal of Earth and Environmental Sciences, 7(2): 109–117

Oroud, I. M. (2018). Global warming and its implications on meteorological and hydrological drought in the southeastern Mediterranean. Environmental Processes. https://doi.org/10.1007/s4071-018-0301-z.

Oroud, I. M., Balling, R. C (2021) The utility of combining optical and thermal images in monitoring agricultural drought in semiarid mediterranean environments, Journal of Arid Environments, 189, https://doi.org/10.1016/j.jaridenv.2021.104499.

Oroud I. M (2022) Derivation of spatially distributed thermal comfort levels using remote sensing, GIS tools and computational methods. Theoretical and Applied Climatology, 148:569–583. https://doi.org/10.1007/ s00704-022-03951-7

Oroud I. M. (2023) The future fate of the Dead Sea: Total disappearance or a dwarfed hypersaline hot lake? Journal of Hydrology, 623, https://doi.org/10.1016/j.jhydrol.2023.129816.

Oroud, I.M. (2024) The implications of climate change on freshwater resources in the arid and semiarid Mediterranean environments using hydrological modeling, GIS tools, and remote sensing. Environmental Monitoring and Assessment, 196, 979. . https://doi.org/10.1007/s10661-024-13139-3

Oroud, I. M., Al-Rousan, N. (2004) Urban Encroachment on Rain-Fed Agricultural Lands in Jordan during the Second Half of the 20th Century, The Arab World Geographer, 7 (3), 165-180, https://doi. 10.5555/arwg.7.3.p57gmvlh24287ntj

Palmer, WC. (1965). Meteorological drought. Office of Climatology Research Paper 45, Weather Bureau, Washington D.C., 58.

Ponce, V. M., & Hawkins, R. (1996). Runoff curve number: Has it reached maturity? Journal of Hydrologic Engineering. https://doi.org/10.1061/(ASCE)1084-0699(1996)1: 1(11)

Ries, F., Schmidt, S., Sauter, M., Lange, J. (2017). Controls on runoff generation along a steep climatic gradient in the Eastern Mediterranean. Journal of Hydrology: Regional Studies, 9, 18–33. https://doi.org/10.1016/j.ejrh.2016.11. 001

Schoener W (2010) Basics of climatological and meteorological observations for GIS applications. In: Carrega P (ed) Geographical Information and Climatology. Wiley-ISTE 288 PP

Small, E., Badger, A., Abolafia-Rosenzweig, R., & Livneh, B. (2018). Estimating soil evaporation using drying rates determined from satellite-based soil moisture records. Remote Sensing. https://doi.org/10.3390/rs10121945

Tabari, H, 2020 Climate change impact on flood and extreme precipitation increases with water availability, Scientific Reports, doi:10.1038/s41598-020-70816-2

Viola, F., Caracciolo, D., Forestieri, A., Pumo, D., & Noto, L. V. (2017). Annual runoff assessment in arid and semiarid Mediterranean watersheds under the Budyko's framework. Hydrological Processes, https://doi.org/10.1002/hyp.11145